RSC Advances

ROYAL SOCIETY OF CHEMISTRY

www.rsc.org/advances

RSC Advances

ARTICLE

Magnetoliposomes based on manganese ferrite nanoparticles as nanocarriers for antitumor drugs

Received 00th January 20xx,
Accepted 00th January 20xx

DOI: 10.1039/x0xx00000x

www.rsc.org/

Ana Rita O. Rodrigues,[a] José M. F. Ramos,[a] I. T. Gomes,[a,b] Bernardo G. Almeida,[a] J. P. Araújo,[b] Maria João R. P. Queiroz,[c] Paulo J. G. Coutinho[a] and Elisabete M. S. Castanheira[a,†]

Manganese ferrite nanoparticles with a size distribution of 26±7 nm (from TEM measurements) were synthesized by the coprecipitation method. The obtained nanoparticles exhibit a superparamagnetic behaviour at room temperature with a magnetic squareness of 0.016 and a coercivity field of 6.3 Oe. These nanoparticles were either entrapped in liposomes (aqueous magnetoliposomes, AMLs) or covered with a lipid bilayer, forming solid magnetoliposomes (SMLs). Both types of magnetoliposomes, exhibiting sizes below or around 150 nm, were found to be suitable for biomedical applications. Membrane fusion between magnetoliposomes (both AMLS and SMLs) and GUVs (giant unilamellar vesicles), the latter used as models of cell membranes, was confirmed by Förster Resonance Energy Transfer (FRET) assays, using a NBD labeled lipid as the energy donor and Nile Red or Rhodamine B-DOPE as the energy acceptor. A potential antitumor thienopyridine derivative was successfully incorporated into both aqueous and solid magnetoliposomes, pointing to a promising application of these systems in oncological therapy, simultaneously as hyperthermia agents and nanocarriers for antitumor drugs.

Introduction

Since their discovery, liposomes have been described as an ideal nanoencapsulation system that protect and transport loaded compounds to the sites of interest.[1-3] In fact, liposomes can overcome many of the problems associated with other systems used in therapy, such as those involving solubility, pharmacokinetics, *in vivo* stability and toxicity.[4,5] However, this system still presents some issues for *in vivo* application, namely its recognition and capture by the immune system[6] and also the location in therapeutic sites for drug release.[7] In order to overcome these problems, magneto-sensitive liposomes have been proposed.[8] The magnetic components allow concentration of the liposomes in the desired area of the patient's organs by magnetic forces, often augmented by magnetic agglomeration.[9-11] This way, a new therapy emerges, involving the guided transport of biologically active substances, most of them toxic and with systemic side effects. The ability to guide transported drugs and focus the active molecules to specific sites in the human body can overcome systemic toxicity problems, allowing a lower drug dosage and a more efficient treatment, not only in cancer but also in other diseases.

Magneto-sensitive liposomes result from the encapsulation of magnetic nanoparticles into liposomes. The so-called magnetoliposomes (MLs) combine the amazing physical properties of these two types of particles and preserve the magnetic properties of the magnetic nanoparticles.[12] This ideal system can be exploited in a great array of biomedical applications. In therapy, the most promising applications of magnetoliposomes are magnetic guided drug delivery and hyperthermia.[13,14] Otherwise, in diagnosis, magnetic nanoparticles have been used as contrast agents in MRI (magnetic resonance imaging).[15]

Magnetic nanoparticles (NPs) of transition metal ferrites (MFe_2O_4, M = Mn, Co, Ni, etc.), having a spinel structure, are of strong interest for biomedical applications. These nanoparticles are remarkable soft-magnetic materials with superparamagnetic behavior and have great properties, such as good chemical stability and mechanical hardness.[16,17] In particular, manganese ferrite NPs have received an increased attention. Their magnetic susceptibility is higher than for other ferrite nanoparticles,[18] suggesting that they may be used in magnetic drug targeting and as an ultrasensitive negative contrast agent in MRI.[19,20] Also, manganese ferrite NPs showed good biocompatibility and slight toxicity against HeLa cells.[21]

The preparation method of magnetic NPs determines their final shape, size distribution, surface chemistry and magnetic properties.[22,23] In this work, manganese ferrite nanoparticles were synthesized by the coprecipitation method. These NPs were either entrapped in liposomes, originating aqueous magnetoliposomes (AMLs), or covered with a lipid bilayer, forming solid

[a] Centro de Física (CFUM), Universidade do Minho, Campus de Gualtar, 4710-057 Braga, Portugal.
[b] IFIMUP/IN - Instituto de Nanociência e Nanotecnologia, R. Campo Alegre, 4169-007 Porto, Portugal.
[c] Centro de Química (CQ/UM), Universidade do Minho, Campus de Gualtar, 4710-057 Braga, Portugal.

[†] Corresponding author; Phone: +351 253604321; Fax: +351 253604061; ecoutinho@fisica.uminho.pt

Electronic Supplementary Information (ESI) available: Size distribution of aqueous and solid magnetoliposomes (obtained by DLS). See DOI: 10.1039/x0xx00000x

magnetoliposomes (SMLs). A potent antitumor heteroaryl-aminothieno[3,2-*b*]pyridine derivative (Figure 1), previously synthesized,[24] was incorporated into both types of magnetoliposomes, keeping in mind future biomedical applications. In fact, magnetoliposomes are promising for dual cancer therapy, both by hyperthermia and anticancer drug delivery, besides the ability to attain magnetic guidance to the therapeutic site of interest.

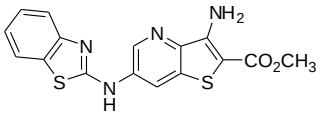

Compound **1**

Fig. 1 Structure of the methyl 3-amino-6-(benzo[*d*]thiazol-2-ylamino)thieno[3,2-*b*]pyridine-2-carboxylate (**1**).

Experimental

All the solutions were prepared using spectroscopic grade solvents and ultrapure water (Milli-Q grade).

Manganese ferrite nanoparticles preparation

Manganese ferrite nanoparticles (NPs) were synthesized by the coprecipitation method, in 5 mL aqueous solution. First, an aqueous solution containing 612 µL of 50% NaOH solution was heated to 90 °C. Then, a mixture containing 500 µL of 0.5 M $MnSO_4.H_2O$ aqueous solution and 500 µL of 1 M $FeCl_3.6H_2O$ aqueous solution was added drop by drop to the previously warmed NaOH solution under magnetic stirring. Manganese nanoparticles were formed after two hours at 90 °C.

Preparation of magnetoliposomes

Aqueous magnetoliposomes (AMLs) resulted from the entrapment of the synthesized magnetic NPs in liposomes. Egg yolk phosphatidylcholine (Egg-PC), from Sigma-Aldrich, was used for lipid vesicle formation. A 10 mM Egg-PC solution in ethanol was injected, under vigorous vortexing, to an aqueous solution of magnetic nanoparticles (ethanolic injection method).[25] Then, the ferrofluid was washed with water and purified by ultracentrifugation to remove all the non-encapsulated NPs.

Solid magnetoliposomes (SMLs) were prepared by the method previously developed by us.[26] First, 10 µL of the synthesized $MnFe_2O_4$ NPs were dispersed in 3 mL of water and centrifuged. Then, the deposited particles were dispersed in 10 µL water in an ultrasonicator for one minute at 189 W, and 3 mL of chloroform were added to the aqueous dispersion of NPs. After vigorous agitation, 165 µL of a 20 mM solution of 1,2-dioleoyl-*sn*-glycero-3-phospho-(1'-*rac*-glycerol) (sodium salt) (DOPG, from Sigma-Aldrich) were added under vortexing, to form the first lipid layer of the SMLs. The particles were washed twice by magnetic decantation with pure water, in order to remove the lipid that was not attached to the NPs. The second lipid layer was then formed by the injection of 165 µL of DOPG (20 mM), under vortexing, in a 3 mL aqueous dispersion of the particles with the first lipid layer. The resulting SMLs were then washed and purified with pure water by centrifugation.

Compound **1** was incorporated into aqueous magnetoliposomes by the co-injection method, as already described for liposomes.[27] In solid magnetoliposomes, compound **1** was incorporated by injection of an ethanolic solution together with the formation of the second lipid layer.

Preparation of Giant Unilamellar Vesicles (GUVs)

Soybean lecithin (*L*-α-Phosphatidylcholine), from Sigma-Aldrich, was used for GUVs preparation, using a procedure previously described.[28,29] 100 µL of soybean lecithin solution (1 mM) were dried under an argon stream to produce a thin and homogeneous lipid film. 40 µL of water were added to the film and it was incubated at 45 °C for 30 minutes. Then, 3 mL of 0.1 M glucose aqueous solution were added and the resulting mixture was again incubated at 37 °C for 2 hours. Finally, after incubation, the GUVs suspension was centrifuged at 14000 *g* for 30 minutes at 20 °C, to remove multilamellar vesicles and lipid aggregates.

Spectroscopic measurements

General methods. Absorption spectra were recorded in a Shimadzu UV-3101PC UV-Vis-NIR spectrophotometer. Fluorescence measurements were performed using a Fluorolog 3 spectrofluorimeter, equipped with double monochromators in both excitation and emission and a temperature controlled cuvette holder. Fluorescence spectra were corrected for the instrumental response of the system.

FRET measurements. Assays of non-specific interaction between magnetoliposomes and models of biological membranes (GUVs) were performed by Förster Resonance Energy Transfer (FRET). The NBD labeled lipids NBD-PE (*N*-(7-nitrobenz-2-oxa-1,3-diazol-4-yl)-1,2-dihexadecanoyl-*sn*-glycero-3-phosphoethanolamine, ammonium salt) or NBD-C_{12}-HPC (1-palmitoyl-2-{12-[(7-nitro-2-1,3-benzoxadiazol-4-yl)amino]hexanoyl}-*sn*-glycero-3-phosphocholine), from Avanti Polar Lipids, were used as the energy donors, while the hydrophobic dye Nile Red (from Fluka) or the labeled lipid Rhodamine B-DOPE (*N*-(lissamine Rhodamine B sulfonyl)-1,2-dioleoyl-*sn*-3-phosphatidylethanolamine (ammonium salt)), from Avanti Polar Lipids, were used as the energy acceptors.

FRET efficiency, Φ_{RET}, defined as the proportion of donor molecules that have transferred their excess energy to acceptor molecules, can be obtained by taking the ratio of the donor integrated fluorescence intensities in the presence of acceptor (F_{DA}) and in the absence of acceptor (F_D) (eqn. 1),[30]

$$\Phi_{\mathrm{RET}} = 1 - \frac{\mathrm{F_{DA}}}{\mathrm{F_D}} \qquad (1)$$

The distance between donor and acceptor molecules can be determined through the FRET efficiency (eqn. 2),

$$r_{\mathrm{AD}} = R_0 \cdot \left[\frac{1-\Phi_{\mathrm{RET}}}{\Phi_{\mathrm{RET}}}\right]^{1/6} \qquad (2)$$

where R_0 is the Förster radius (critical distance), that can be obtained by the spectral overlap, J(λ), between the donor emission and the acceptor absorption, according to equations (3) and (4) (with R_0 in Å, λ in nm, $\varepsilon_A(\lambda)$ in M^{-1} cm^{-1}),[30]

$$R_0 = 0.2108\left[k^2\Phi_D^0 n^{-4} J(\lambda)\right]^{1/6} \quad (3)$$

$$J(\lambda) = \int_0^\infty I_D(\lambda)\varepsilon_A(\lambda)\lambda^4 d\lambda \quad (4)$$

where $k^2 = 2/3$ is the orientational factor assuming random orientation of the dyes, Φ_D^0 is the fluorescence quantum yield of the donor in the absence of energy transfer, *n* is the refraction index of the medium, $I_D(\lambda)$ is the fluorescence spectrum of the donor normalized so that $\int_0^\infty I_D(\lambda)d\lambda = 1$, and $\varepsilon_A(\lambda)$ is the molar absorption coefficient of the acceptor.

The fluorescence quantum yield, Φ_s, of the energy donor (the dye NBD) in magnetoliposomes was determined by the standard method (equation 5),[31,32]

$$\Phi_s = \left[\left(A_r F_s n_s^2\right)/\left(A_s F_r n_r^2\right)\right]\Phi_r \quad (5)$$

where *A* is the absorbance at the excitation wavelength, *F* the integrated emission area and *n* is the refraction index of the solvents. Subscripts refer to the reference (r) or sample (s) compound. The absorbance value at excitation wavelength was always less than 0.1, in order to avoid inner filter effects. The NBD-C_{12}-HPC fluorescent labeled lipid incorporated in lipid membranes was used as reference, Φ_r=0.32 at 25 ºC, as reported by Invitrogen.[33]

Fluorescence anisotropy measurements. The steady-state fluorescence anisotropy, *r*, is calculated by

$$r = \frac{I_{VV} - GI_{VH}}{I_{VV} + 2GI_{VH}} \quad (6)$$

where I_{VV} and I_{VH} are the intensities of the emission spectra obtained with vertical and horizontal polarization, respectively (for vertically polarized excitation light), and $G = I_{HV}/I_{HH}$ is the instrument correction factor, where I_{HV} and I_{HH} are the emission intensities obtained with vertical and horizontal polarization (for horizontally polarized excitation light).

Structural characterization

Transmission Electron Microscopy (TEM). HR-TEM images of manganese ferrite nanoparticles and solid magnetoliposomes were recorded using a Transmission Electron Microscope JEOL JEM 2010F operating at 200 kV coupled to an Electron Dispersive Spectroscopic analyzer (EDS) at C.A.C.T.I (Centro de Apoio Científico e Tecnolóxico á Investigación), Vigo, Spain. A drop of the sample was placed onto a TEM copper grid with Formvar/Carbon (ref. S162-4 from Agar Scientific), held by tweezers and left to dry. The processing of TEM images was performed using ImageJ software. It consisted in enhancing local contrast followed by manual selection of particles. The area of each particle allowed an estimation of its size. The resulting histograms were fitted to Gaussian distributions.

X-Ray Diffraction (XRD) and DLS measurements. X-Ray Diffraction (XRD) analyses were performed using a conventional Philips PW 1710 diffractometer, operating with Cu K_α radiation, in a Bragg-Brentano configuration.

The mean diameter and size distribution of the magnetic liposomes were measured using a Dynamic Light Scattering (DLS) equipment (NANO ZS Malvern Zetasizer) at 25 °C, using a He-Ne laser of 633 nm and a detector angle of 173°. Five independent measurements were performed for each sample. The data analysis was performed using the methodology previously described.[34]

Magnetic measurements

General methods. Magnetic measurements were performed at room temperature in a Superconducting Quantum Interference Device (SQUID) magnetometer (Quantum Design MPMS5XL), using applied magnetic fields up to 5.5 T.

Temperature dependence of the magnetization and magnetic hysteresis cycles. The temperature dependence of the magnetization was measured in the temperature range from 5 K to 380 K. The curves were obtained by initially cooling the sample under an applied magnetic field of *H* = 100 Oe (field cooled, *FC*) and then measuring its magnetization with increasing temperature (applied field of *H* = 50 Oe). Subsequently, after reaching 380 K, the sample was re-cooled, this time with no applied magnetic field (zero-field-cooled, *ZFC*) and the magnetization measurements were again performed with increasing temperature, under the same magnetic field of *H* = 50 Oe. From the behavior of the *FC* and *ZFC* curves, the blocking temperature (T_B) of the superparamagnetic nanoparticles can be obtained.[35] The magnetization hysteresis loop measurements were made by fixing the temperature and measuring the magnetization at a series of different applied magnetic fields. This type of study gives information about the maximum magnetization and the degree at which the sample remains magnetized when the applied field is removed, and how easily the sample magnetization can be reversed, the so-called coercive field.

Results and discussion

Nanoparticles characterization

XRD analysis. XRD measurements confirm the synthesis of the manganese ferrite NPs (Figure 2). No calcination was required to obtain a crystalline phase (Figure 2C). However, the absence of thermal treatment results in a significant amorphous background in the XRD pattern. This background disappears upon thermal treatment at 800 °C, but originates the presence of a hematite phase (Figure 2D). The synthesis conditions are especially important, as changing the reaction time from 2 hours to 6 hours made the sample amorphous (Figure 2A). This state remained upon calcination at 500 °C and 600 °C. Treatment at 700 or 800 °C allowed the crystallization of the manganese ferrite phase, but with a much higher percentage of hematite (Figure 2B).

All the characteristic peaks for a pure crystalline phase of manganese ferrite spinel,[36] marked by their indices, are shown in Figure 2. Rietveld analysis using a background defined by linear interpolation between a set of points at constant scattering angles but with fitted intensities resulted in good fits, allowing an estimation of sample composition and particle size. Table 1 summarizes the main results of the Rietveld analysis of the obtained samples, with and without thermal treatment at 800 °C.

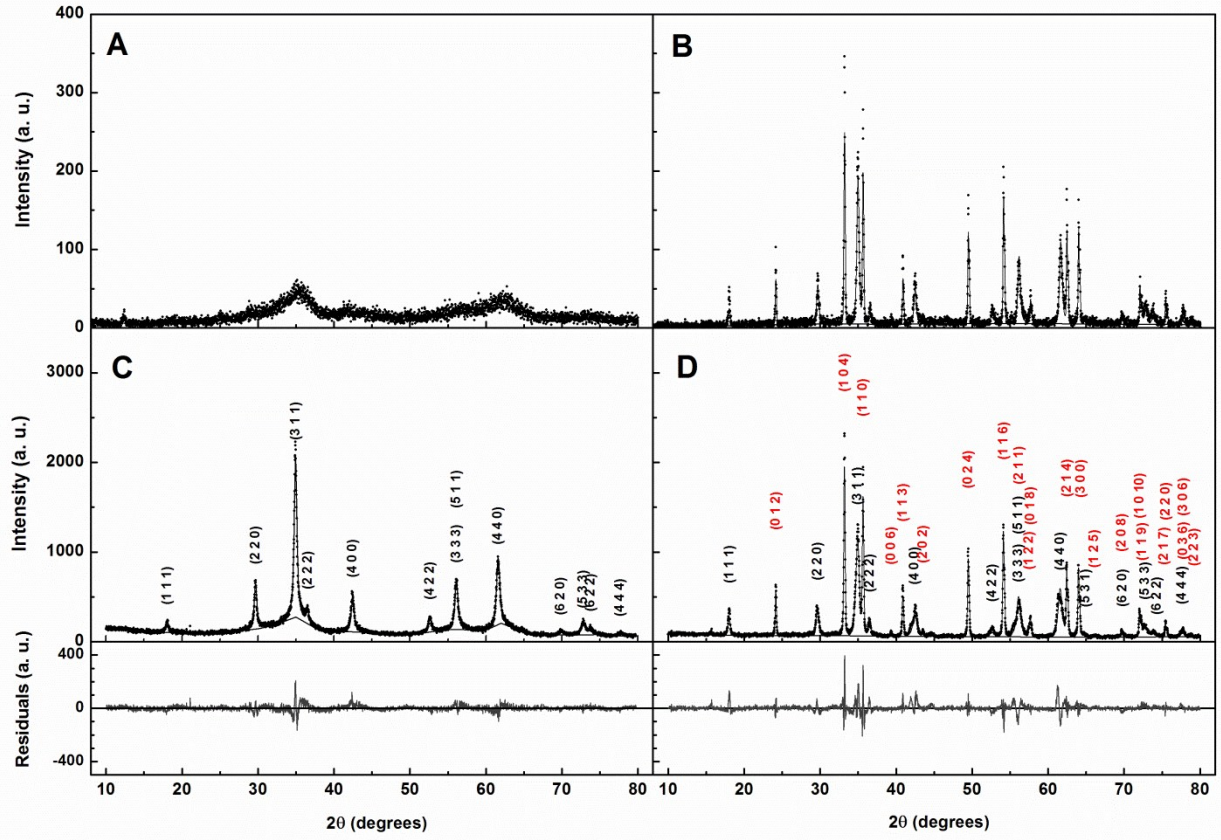

Fig. 2 XRD pattern of the $MnFe_2O_4$ NPs. Left: Without thermal treatment. Right: Calcinated at 800 °C. **A** and **B**: Synthesis time of 6 hours. **C** and **D**: Synthesis time of 2 hours and results of Rietveld analysis ($MnFe_2O_4$: space group Fd-3m:2 (227); CIF 1528316; Fe_2O_3: space group R-3 2/c (167); CIF 9000139).

Table 1. Selected Rietveld analysis parameters.

Reaction time	Calcination temperature	Phase	Fraction (%)	Overall temperature B factor	Size (nm)	R_f	χ^2
2 h	none	$MnFe_2O_4$	100	-0.18	16.5	4.74	1.69
		Fe_2O_3	---	---	---	---	
2 h	800 °C	$MnFe_2O_4$	55	2.88	13.1	5.98	3.09
		Fe_2O_3	45	1.84	140	4.24	
6 h	700 °C	$MnFe_2O_4$	46	1.61	14	14.6	1.54
		Fe_2O_3	54	0.95	252	5.36	
6 h	800 °C	$MnFe_2O_4$	53	0.59	25	15.3	1.60
		Fe_2O_3	47	-0.25	345	7.69	

Calcination treatment at a higher temperature of 900 °C results in huge variations in the XRD spectrum which was then dominated by the presence of Mn_2O_3 and hematite phases, with only traces of manganese ferrite. The size estimation shown in Table 1 is a lower limit, as the XRD peak broadening was considered to arise only from size effects. Inclusion of strain does not improve significantly the fit of the experimental data and originates higher size estimates. For example, in case of the data in Figure 2C (2 h synthesis time without thermal treatment), a maximum strain value of 0.022% corresponds to a size of 25.1 nm and the χ^2 and R_f values decrease to 1.67 and 4.53, respectively. From these XRD results, the sample obtained with 2 hours reaction time and without thermal treatment was selected for further characterization and for the preparation of magnetoliposomes.

UV-Visible Absorption Spectra. Figure 3 displays the UV-Visible absorption spectrum of the synthesized manganese ferrite NPs. The optical band gap can be estimated using a Tauc plot,[37] which corresponds to the following equation:

$$(\alpha h\nu)^{1/n} \propto (h\nu - E_g) \qquad (7)$$

where α is the absorption coefficient that is proportional to the absorbance value and E_g is the optical band gap. The value of *n* depends on the nature of the transition, being 1/2 for an indirect band gap and 2 for a direct one.

A linear relation was only obtained for *n*=1/2 which means that $MnFe_2O_4$ behaves as an indirect semiconductor. This was already reported by Rafique *et al.*[38] with a band gap of 0.98 eV. From Figure 3, a similar value of 1.08 eV was calculated.

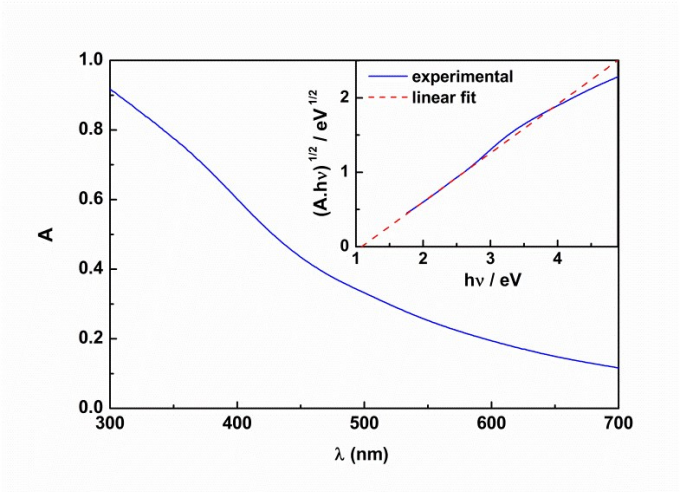

Fig 3 UV-Visible absorption spectra of $MnFe_2O_4$ nanoparticles synthesized by the coprecipitation method. Inset: Tauc plot.

TEM images and elemental analysis. TEM images revealed that the synthesized $MnFe_2O_4$ NPs are generally of small size, with a few larger particles. Particle sizes on the order of tens of nanometers (Figure 4), with a size distribution of 26±7 nm, were obtained from the histogram (C) of image A. From image 4B, it was possible to obtain an interlattice plane distance of 0.49 nm, which corresponds to the (111) diffraction plane. EDAX elemental analysis confirmed the presence of uniform distribution of Mn, Fe and O elements for this type of ferrite nanoparticles (Figure 4D and Table 2). The high copper content (Figure 4D) is due to the use of copper grids.

Magnetic properties. Manganese ferrite nanoparticles are soft ferromagnetic particles and their magnetic behavior depends on the synthesis method and particle size.[22,23] Figure 5 shows the hysteresis loop of $MnFe_2O_4$ NPs at room temperature. A very small hysteresis is observed, with a coercive field of 6.3 Oe. The presence of superparamagnetic behavior can be related to the magnetic squareness value of the hysteresis cycle, which is the ratio between the residual magnetizations (M_r) and the saturation magnetization (M_s). Magnetic squareness values indicative of superparamagnetism are of the order or below 0.1, meaning the loss of more than 90% of the magnetization removal of the applied magnetic field.[39,40] Here, the obtained magnetic squareness value of the nanoparticles is 0.016, which indicates that the synthesized $MnFe_2O_4$ NPs present a superparamagnetic behavior at room temperature. Additionally, the magnetization of $MnFe_2O_4$ NPs does not saturate up to the maximum field that was applied, as shown on figure 5, reaching 36 emu/g at an applied field of 5 T.

For a superparamagnet, the temperature dependence of the zero-field-cooling and field-cooling magnetization curves presents a different behavior. Starting from the low temperatures on the *ZFC* curve, as temperature increases the blocked magnetic moments align with the applied measuring magnetic field, leading to an initial increase of the sample magnetization. However, as soon as thermal fluctuations are able to allow the moments to overcome the magnetic anisotropy energy barrier, the thermal randomization of the intra-particles magnetic moments produces a subsequent decrease of the magnetization curve, with increasing temperature. In this way, the zero-field-cooling curve peak corresponds to the sample blocking temperature[41] and here a blocking temperature of T_B ~ 316 K, was obtained for $MnFe_2O_4$ nanoparticles.

On the other hand, on the *FC* curve, the magnetic moments were initially forced to be aligned with the magnetic field imposed during cooling. This then gives a significant overall magnetization at low temperatures, as seen on the *FC* curve of Figure 6, which monotonically decreases with increasing temperature. Below T_B, the magnetic nanoparticles show ferromagnetic behavior, as thermal fluctuations are not enough to randomize the intra-particles magnetic moments. Above the blocking temperature, NPs show superparamagnetic properties and the *ZFC* and *FC* curves are expected to show the same magnetization decreasing trend with increasing temperature. The observed difference between the *ZFC* and *FC* above T_B is related with the size dispersion of the nanoparticles.

For an ensemble of superparamagnetic particles above the blocking temperature, the magnetization can be described by the Langevin function[41]

$$M(H,T) = N\mu L\left(\frac{\mu H}{K_B T}\right) = N\mu\left(\coth\left(\frac{\mu H}{K_B T}\right) - \frac{K_B T}{\mu H}\right) \qquad (7)$$

where μ *is* the particle magnetic moment, k_B is the Boltzmann constant, *T* is the absolute temperature, *N* is the number of particles per volume and *H* is the applied magnetic field.

Table 2. Atomic percentages of individual elements in $MnFe_2O_4$ nanoparticles.

Element	EDAX atomic (%)	Calculated atomic (%)
Mn	13.8	14.3
Fe	23.6	28.6
O	62.6	57.1

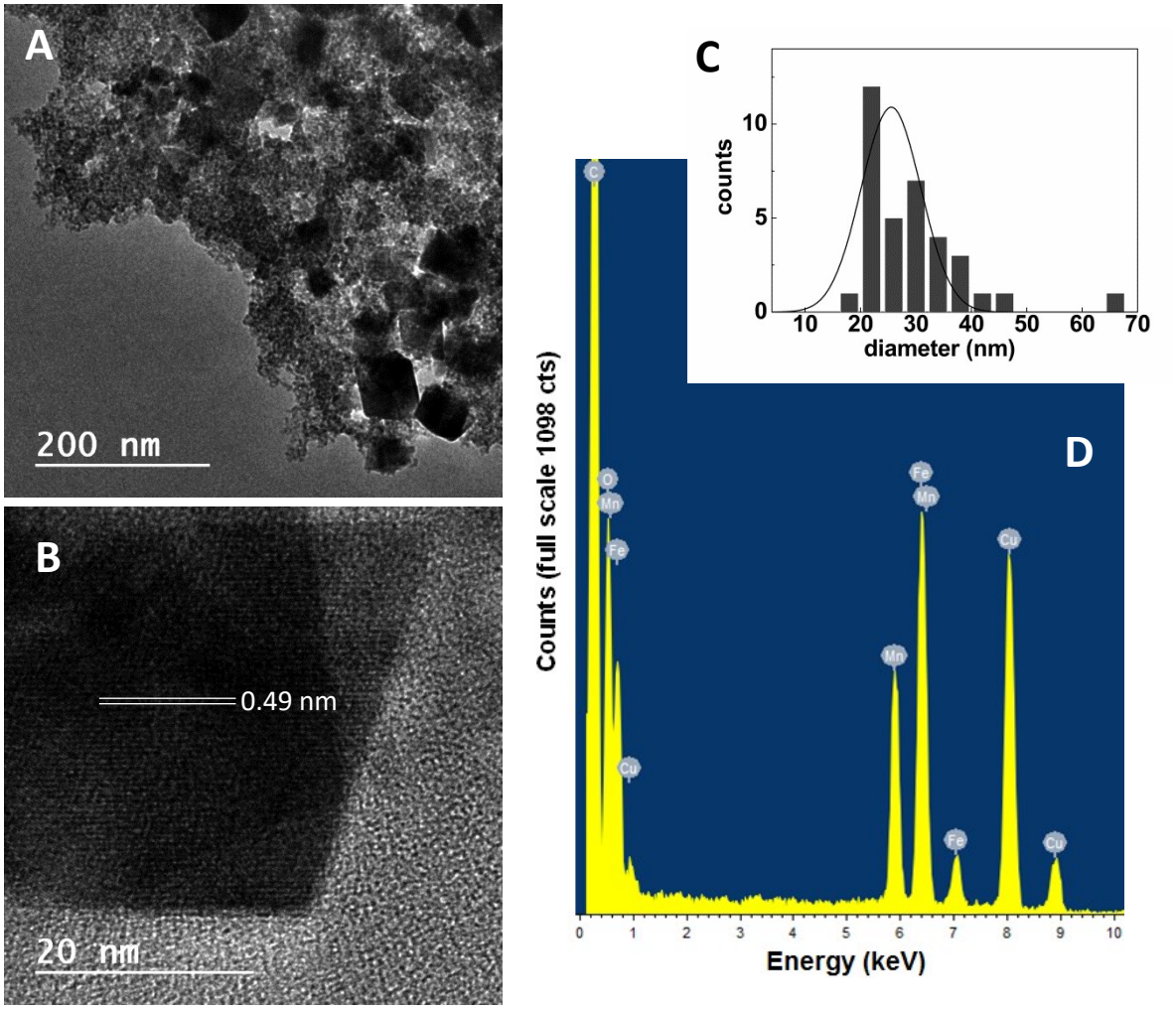

Fig. 4 A, B: TEM images of the synthesized $MnFe_2O_4$ NPs at different amplifications. **C**: Particles size histogram of image **A** and fitting to a Gaussian distribution. **D**: EDAX elemental analysis of area corresponding to image **A**.

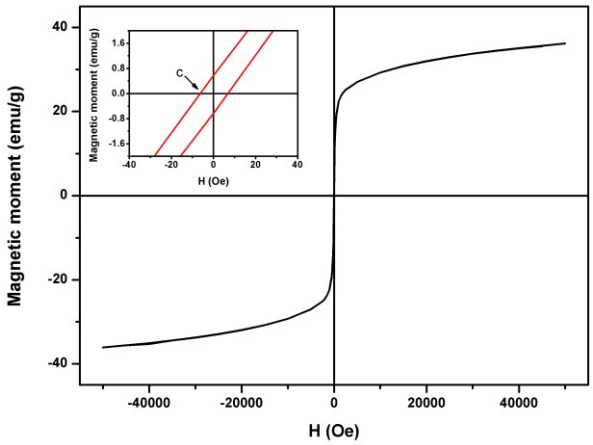

Fig. 5 Magnetization hysteresis loop of $MnFe_2O_4$ NPs measured at room temperature. Inset: Enlargement of the loop, in the low field region.

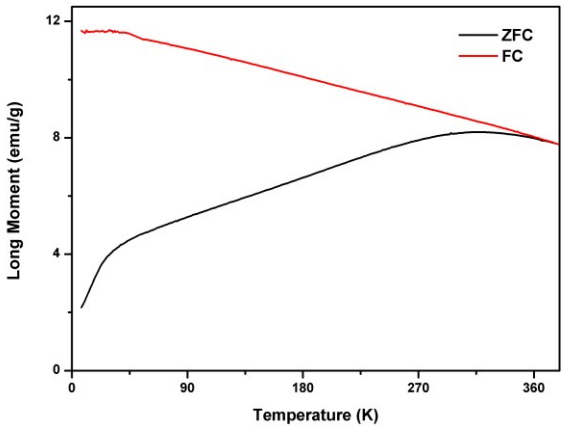

Fig. 6 *ZFC* and *FC* magnetization curves of manganese ferrite nanoparticles.

The magnetization hysteresis cycles were fitted to equation (7), in order to determine the particle magnetic moment, μ. Considering a magnetic moment of $\mu_{MnFe_2O_4} = 4.6\mu_B$ per $MnFe_2O_4$,[41] the number of formula units per particle can be obtained by dividing the fitted particle magnetic moment by $\mu_{MnFe_2O_4}$. The particle radius can be estimated by assuming spherical particles, with a density value of 4.87 g/cm^3.[42] Table 3 shows the results obtained for the fitting of equation (7) to the hysteresis loops. The value determined for diameter is of the order of 14 nm. The high value of R^2 (Table 3) indicates that the experimental data closely follow a Langevin function, as expected for superparamagnetic nanoparticles. The obtained nanoparticle diameter is consistent with the corresponding values obtained from the XRD results, indicating a well ordered manganese ferrite phase without significant surface oxidation or secondary residual phases. Here, the higher magnetization and lower coercivity as compared, e.g., to nickel ferrite nanoparticles,[26] makes the prepared manganese ferrite nanoparticles promising candidates for biomedical applications.

Characterization of magnetoliposomes

DLS and TEM measurements. Two types of magnetoliposomes were synthesized, aqueous magnetoliposomes (AMLs) and solid magnetoliposomes (SMLs). Dynamic Light Scattering (DLS) measurements revealed that aqueous magnetoliposomes of egg phosphatidylcholine (Egg-PC) with entrapped manganese ferrite nanoparticles have diameters of 82±13 nm (size distribution in Figure S1 of Supplementary Information). These values are in accordance with previous results reported for egg lecithin-based liposomes without nanoparticles[34,43] showing that, as previously observed for nickel ferrite NPs,[26] the manganese ferrite nanoparticles have a very small influence on the size of aqueous magnetoliposomes. Neat Egg-PC aqueous magnetoliposomes containing lauric acid coated $MnFe_2O_4$ nanoparticles were previously prepared by Pradhan and coworkers,[44] using two different techniques, thin film hydration and double emulsion, resulting in magnetoliposomes of *ca.* 300 nm diameter. This size is significantly larger than the one obtained here using the ethanolic injection method. Pradhan *et al.*[44] also reported that PEGylated Egg-PC:Cholesterol 2:1 AMLs prepared by thin film hydration (with diameter around 188 nm) are the most promising systems (amongst a series of different Egg-PC:Chol compositions) for hyperthermia treatment of cancer.

Solid magnetoliposomes (SMLs) were obtained by coverage of a cluster of manganese ferrite NPs by the phospholipid DOPG, using the method previously developed for Ni ferrite NPs.[26] This method already proved to originate SML structures, with a lipid bilayer surrounding a cluster of magnetic nanoparticles.[26]

TEM images revealed that the synthesized SMLs have diameters slightly above 100 nm (Figure 7) therefore being suitable for biomedical applications. Dynamic Light Scattering measurements allowed determining a hydrodynamic diameter of 152±24 nm, roughly in accordance with TEM data (DLS size distribution is shown in Figure S2 of Supplementary Information).

AMLs interaction with model membranes. The non-specific interaction of aqueous magnetoliposomes (AMLs) with models of cell membranes (giant unilamellar vesicles, GUVs) was evaluated by Förster Resonance Energy Transfer (FRET). For that purpose, the labeled lipid NBD-C_{12}-HPC and the hydrophobic dye Nile Red were both incorporated in the lipid bilayer of the aqueous magnetoliposomes, the NBD moiety acting as the energy donor and the hydrophobic dye Nile Red as the energy acceptor.[45-49] If the donor-acceptor distance is below 100 Å,[30] improved FRET efficiency is expected, as the spectral overlap between the donor fluorescence band and the acceptor absorption is high (Figure 8A, inset).

When the aqueous magnetoliposomes interact with model membranes (GUVs), if fusion occurs, a larger membrane is originated and an increase in the donor-acceptor distance is expected, with a corresponding decrease in the energy transfer efficiency. Fluorescence spectra of Egg-PC AMLs, before and after interaction with GUVs, were measured exciting only the donor (NBD). Before interaction with GUVs, two emission bands are clearly observed. The first (λ_{max}=550 nm) corresponds to NBD-C_{12}-HPC emission and the second (λ_{max}=630 nm) to Nile Red emission, that results from the energy transfer of excited NBD molecules to Nile Red. After interaction with GUVs, an increase in the NBD (donor) emission band and a decrease of the Nile Red (acceptor) fluorescence band is observed.

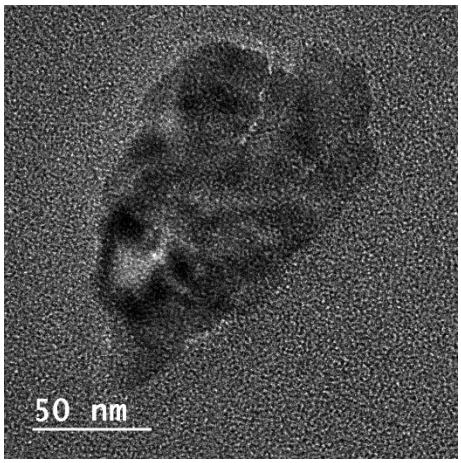

Fig. 7 TEM image of the solid magnetoliposomes (SMLs) containing $MnFe_2O_4$ NPs.

Table 3. Magnetization saturation (M_s), mass (m) and size (d) of the synthesized manganese ferrite nanoparticles.

Sample	R^2	M_s (emu/g)	m (g)	V (cm^3)	d (nm)
$MnFe_2O_4$	0.9879	31.8	6.98×10^{-18}	1.43×10^{-18}	13.97

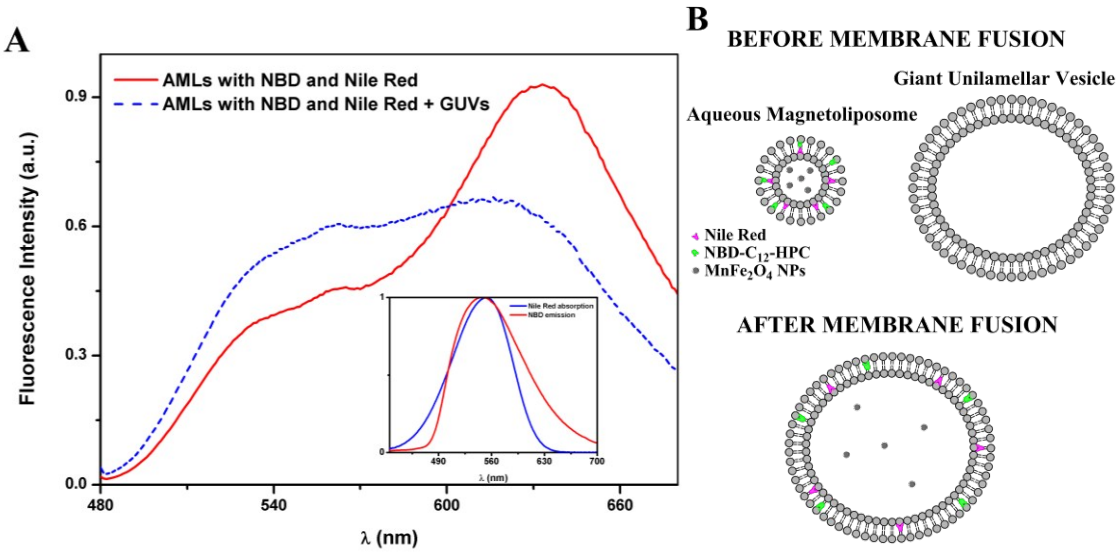

Fig. 8 A. Fluorescence spectra (λ_{exc}=400 nm) of AMLs of egg lecithin and $MnFe_2O_4$ NPs containing both NBD-C_{12}-HPC and Nile Red, before and after interaction with GUVs. Inset: Spectral overlap (spectra are normalized) between the fluorescence emission of the donor (NBD-C_{12}-HPC) and the absorption of the acceptor (Nile Red). **B.** Schematic representation of membrane fusion between AMLs and GUVs.

These results are similar to the ones previously observed for AMLs based on $NiFe_2O_4$ nanoparticles[26] and confirm membrane fusion between the two systems, AMLs and GUVs (scheme in Figure 8B). Therefore, AMLs based on manganese ferrite nanoparticles are promising as magnetic nanocarriers for both hydrophilic and hydrophobic drugs, as they can be guided with a magnetic field and can release the encapsulated drugs by fusion with the cell membranes.

SMLs formation and interaction with model membranes. Solid magnetoliposomes (SMLs) are expected to present a better magnetic response when compared with AMLs, because SMLs keep almost the same magnetic properties as the neat nanoparticles.[50] Besides, it was shown that AMLs display poor magnetic characteristics, similar to those of the aqueous ferrofluid.[51]

The method previously developed for the synthesis of SMLs of calcinated nickel ferrite nanoparticles[26] was also used here with manganese ferrite NPs. The formation of a DOPG bilayer around $MnFe_2O_4$ NPs was investigated by FRET assays. For that purpose, the NDB labeled lipid NBD-C_6-HPC was included in the second lipid layer of the SMLs (NBD acting as the energy donor), while the labeled lipid Rhodamine B-DOPE (energy acceptor) was included in the first lipid layer. The emission of SMLs containing both donor and acceptor labeled lipids was measured exciting only the donor NBD, and was compared with the emission of SMLs labeled with only the energy donor (Figure 9). Comparing the fluorescence spectra of the two systems, a decrease in the NBD emission band and the presence of a pronounced Rhodamine B emission is observed in SMLs containing both fluorophores, evidencing the energy transfer from the excited NBD to Rhodamine.

A FRET efficiency of 86% was calculated from eqn. (1) to (4), with a corresponding donor-acceptor distance (*r*) of 3.9 nm. Typically, a cell membrane presents a thickness of 7 to 9 nm.[52] Therefore, it can be concluded that the labeled lipids Rh-DOPE and NBD-C_6-HPC are located in the first and second lipid layer, respectively, around the nanoparticle clusters, confirming the synthesis of the solid magnetoliposomes.

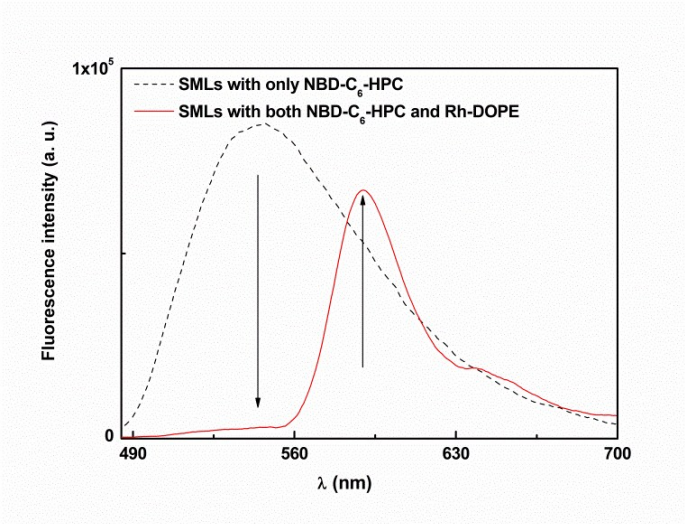

Fig. 9 Fluorescence spectra (λ_{exc} = 470 nm, no rhodamine excitation) of SMLs covered with DOPG labeled with only NBD-C_6-HPC and SMLs labeled with both NBD-C_6-HPC and rhodamine B-DOPE.

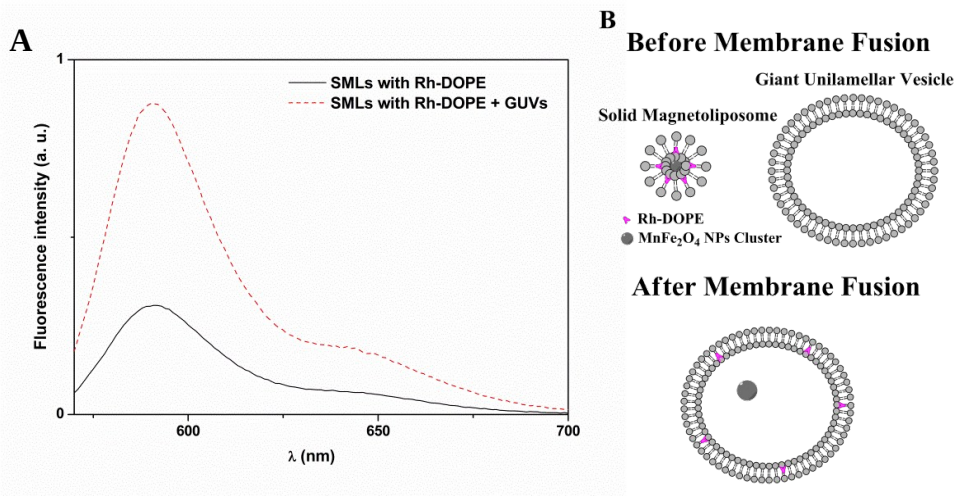

Fig. 10 A. Fluorescence spectra (λ_{exc}=560 nm) of SMLs based on $MnFe_2O_4$ NPs covered with DOPG labeled with Rhodamine B-DOPE before and after interaction with GUVs. **B.** Schematic representation of the fusion between the GUVs and labeled SMLs.

For the study of SMLs interaction with model membranes (GUVs), the same labeled lipids were both included in the SMLs membrane. However, upon interaction with GUVs, FRET measurements did not allow observing the decrease of energy transfer by the increase in NBD (donor) emission band and the decrease of Rhodamine (acceptor) fluorescence band after interaction. Differently, a significant increase in both donor (NBD) and acceptor (Rhodamine) emission bands was detected (data not shown). One possible explanation for the rise in both emission bands upon interaction with GUVs is a quenching effect of both donor and acceptor emissions by the cluster of $MnFe_2O_4$ nanoparticles in SMLs. Upon fusion with model membranes (GUVs), the distance between the NPs cluster and the fluorescent moieties in the SMLs membrane would increase, leading to an unquenching effect. To confirm this hypothesis, the SMLs membrane was labeled only with Rhodamine B-DOPE, and the emission spectrum was measured before and after interaction with GUVs (Figure 10). After interaction, an increase in the fluorescence emission was observed (Figure 10A), confirming the unquenching effect caused by the increase of the distance between NPs and the rhodamine moiety. These results indicate that the SMLs can also fuse with cell membranes and are promising as nanocarrier systems for hydrophobic drugs, which can be released upon fusion with cell membranes.

Incorporation of a potential antitumor drug. The thienopyridine derivative **1** (Figure 1) presents very low growth inhibitory concentration values (GI_{50}), between 3.5 and 6.9 μM, when tested *in vitro* against several human tumor cell lines, namely MCF-7 (breast adenocarcinoma), A375-C5 (melanoma) and NCI-H460 (non-small cell lung cancer) and was the most active of a series of analogues.[24] Moreover, this compound has shown a very low affinity for the multidrug resistance protein MDR1,[27] being promising as an anticancer agent in oncological therapy, as MDR1 promotes drug resistance in cells.

Compound **1** was incorporated in both AMLs and SMLs of Mn ferrite NPs. Figure 11 shows the emission spectra of **1** in AMLs, SMLs and liposomes (without magnetic nanoparticles and with the same concentration of compound). It is possible to observe a quenching effect of the compound emission by the magnetic nanoparticles, proving the incorporation of the thienopyridine derivative in these magnetic nanocarriers. As expected, the fluorescence quenching is much more pronounced for solid magnetoliposomes, where the magnetic nanoparticles are closer to the antitumor compound, which is located mainly in the lipid membrane.[27] Fluorescence anisotropy measurements (Table 4) confirm that this compound is fully incorporated in both types of magnetoliposomes, located mainly in the lipid bilayer, as anisotropy values are similar to those previously determined in liposomes of the same lipids.[27]

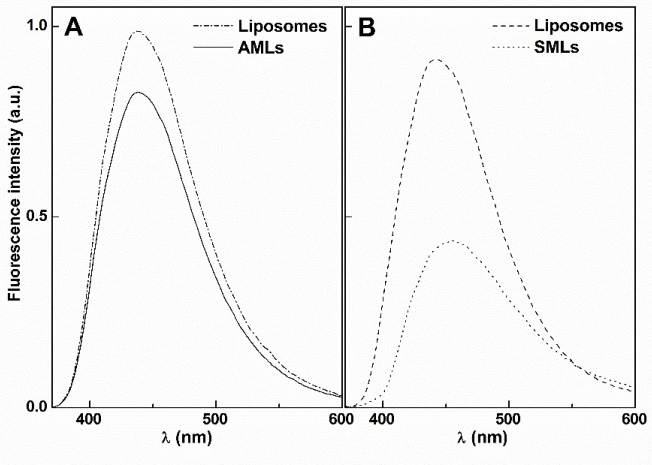

Fig. 11 Fluorescence spectra (λ_{exc}=360 nm) of compound **1** (3×10^{-6} M) in liposomes and magnetoliposomes of Mn ferrite nanoparticles. **A.** Liposomes and AMLs of the phospholipid Egg-PC; **B.** Liposomes and SMLs of the phospholipid DOPG.

Table 4. Steady-state fluorescence anisotropy (*r*) values for antitumor compound **1** in liposomes (without NPs), aqueous magnetoliposomes (AMLs) and solid magnetoliposomes (SMLs).

	Lipid formulation	Temperature	*r*
Liposomes	Egg-PC (100%) [27]	25 °C	0.176
	Egg-PC:Ch (7:3) [27]	25 °C	0.137
	DPPC (100%) [27]	25 °C	0.256
		55 °C	0.130
	DOPG (100%)	25 °C	0.181
		55 °C	0.143
AMLs	Egg-PC (100%)	25 °C	0.171
	Egg-PC:Ch (7:3)	25 °C	0.152
	DPPC (100%)	25 °C	0.201
		55 °C	0.136
SMLs	DOPG (100%)	25 °C	0.189
		55 °C	0.127

Interaction with model membranes (GUVs) was also investigated for both types of magnetoliposomes with incorporated compound **1**. In the case of AMLs, a FRET assay was performed, where the magnetoliposomes containing the antitumor drug **1** were labeled with NBD-PE, compound **1** acting as the energy donor and the NBD moiety as the energy acceptor. It was possible to confirm membrane fusion between AMLs and GUVs, proved by the diminution of FRET process from the drug to NBD (Fig. 12A).

Otherwise, for SMLs, taking into account the fluorescence quenching caused by the presence of Mn ferrite NPs, compound **1** was incorporated in solid magnetoliposomes and the emission spectrum of compound **1** was measured before and after interaction with GUVs (Fig. 12B). The unquenching effect observed after interaction with GUVs proves the membrane fusion between SMLs and the model membranes.

Therefore, the magnetoliposomes here prepared are promising as carriers for this antitumor compound. These results show that both aqueous and solid drug-loaded magnetoliposomes are promising as therapeutic agents, as they can be guided with a magnetic field to the therapeutic site and can release the loaded drug by fusion with the cell membrane.

Conclusions

In this work, small manganese ferrite nanoparticles were synthesized by coprecipitation method. Superparamagnetic properties were obtained for the $MnFe_2O_4$ NPs, with maximum magnetization of 36 emu/g at 5 T applied field and coercivity of 6.3 Oe.

The manganese ferrite nanoparticles were successfully encapsulated into liposomes (forming aqueous magnetoliposomes, AMLs) or covered by a lipid bilayer (solid magnetoliposomes, SMLs). FRET measurements pointed to membrane fusion between the magnetoliposomes (AMLs and SMLs) and models of cell membranes.

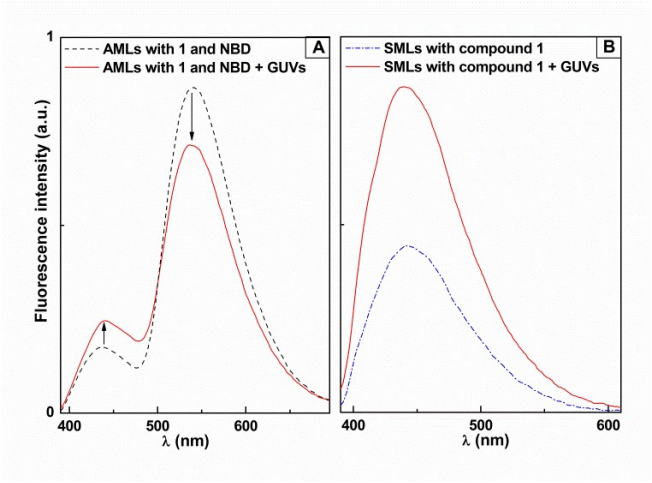

Fig. 12 A. Fluorescence spectra (λ_{exc}=360 nm) of AMLs of Egg-PC and $MnFe_2O_4$ NPs containing both NBD-PE (4×10^{-6} M) and compound **1** (4×10^{-6} M), before and after interaction with GUVs. **B.** Fluorescence spectra (λ_{exc}=360 nm) of compound **1** (4×10^{-6} M) in SMLs of DOPG and $MnFe_2O_4$ NPs before and after interaction with GUVs.

A potent antitumor thienopyridine derivative was successfully incorporated in both AMLs and SMLs. To our knowledge, it is the first time that solid magnetoliposomes based on manganese ferrite nanoparticles were prepared and evaluated as anticancer drug carriers.

These results are promising for future drug delivery applications of anticancer drugs using magnetoliposomes of $MnFe_2O_4$ nanoparticles simultaneously as drug nanocarriers and hyperthermia agents.

Acknowledgements

This work was supported by FEDER through the COMPETE/QREN/EU Program and by the Portuguese Foundation for Science and Technology (FCT) in the framework of the Strategic Projects of CFUM [PEst-C/FIS/UI0607/2013 (F-COMP-01-0124-FEDER-022711)] and CQ/UM [PEst-C/QUI/UI0686/2013 (FCOMP-01-0124-FEDER-022716)].

FCT, POPH-QREN and FSE are acknowledged for the PhD grant of A. R. O. Rodrigues (SFRH/BD/90949/2012) and for financial support to MAP-Fis PhD Programme.

Notes and references

1 M. Mezei and V. Gulasekharam, Liposomes – a selective drug delivery system for the topical route of administration, *Life Sci.,* 1980, **26**, 1473-1477.

2 R. L. Juliano, Liposomes as a drug delivery system. *Trends Pharm. Sci.,* 1981, **2**, 39-41.

3 G. Poste, C. Cucana, A. Raz, P. Bugelski, R. Kirsj and I. J. Fidler, Analysis of the fate of systemically administered liposomes and implication for their use in drug delivery, *Cancer Res.*, 1982, **42**, 1412-1422.

4 T. L. Andresen, S. S. Jensen and K. Jorgensen, Advanced strategies in liposomal cancer therapy: Problems and prospects of active and tumor specific drug release, *Prog. Lipid Res*., 2005, **44**, 68-97.
5 N. A. Ochekpe, P. O. Olorunfemi and N. C. Ngwuluka, Nanotechnology and Drug Delivery, Part 1: Background and Applications, *Trop. J. Pharm. Res.,* 2009, **8**, 265-274.
6 Y. Seow and M. J. Wood, Biological Gene Delivery Vehicles: Beyond Viral Vectors, *Mol. Ther.*, 2009, **17**, 767-777.
7 T. M. Allen and P. R. Cullis, Liposomal drug delivery systems: From concept to clinical applications, *Adv. Drug Delivery Rev.,* 2013, **65**, 36-48.
8 M. M. Elmi and M. N. Sarbolouki, A simple method for preparation of immuno-magnetic liposomes, *Int. J. Pharm.*, 2001, **215**, 45-50.
9 A. A. Kuznetsov, V. I. Filippov, O. A. Kuznetsov, V. G. Gerlivanov, E. K. Dobrinsky and S. I. Malashin, New ferro-carbon adsorbents for magnetically guided transport of anti-cancer drugs, *J. Magn. Magn. Mater.*, 1999, **194**, 22-30.
10 O. A. Kuznetsov, N. A. Brusentsov, A. A. Kuznetsov, N. Y. Yurchenko, N. E. Osipov and F. S. Bayburtskiy, Correlation of the coagulation rates and toxicity of biocompatible ferromagnetic microparticles, *J. Magn. Magn. Mater.,* 1999, **194**, 83-89.
11 A. A. Kuznetsov, V. I. Filippov, R. N. Alyautdin, N. L. Torshina and O. A. Kuznetsov, Application of magnetic liposomes for magnetically guided transport of muscle relaxants and anti-cancer photodynamic drugs, *J. Magn. Magn. Mater*., 2001, **225**, 95-100.
12 K. Nahar, S. Absar, B. Patel and F. Ahsan, Starch-coated magnetic liposomes as an inhalable carrier for accumulation of fasudil in the pulmonary vasculature, *Int. J. Pharm.*, 2014, **464**, 185-195.
13 G. Béalle, R. Di Corato, J. Kolosnjaj-Tabi, V. Dupuis, O. Clément, F. Gazeau, C. Wilhelm and C. Ménager, Ultra Magnetic Liposomes for MR Imaging, Targeting, and Hyperthermia, *Langmuir*, 2012, **28**, 11834-11842.
14 A. Hervault and N. T. K. Thanh, Magnetic nanoparticle-based therapeutic agents for thermo-chemotherapy treatment of cancer, *Nanoscale*, 2014, **6**, 11553-11573.
15 H-J. Weinmann, W. Ebert, B. Misselwitz and H. Schmitt-Willich, Tissue-specific MR contrast agents. *Eur. J. Radiol*., 2003, **46**, 33-44.
16 C. Pereira, A. M. Pereira, C. Fernandes, M. Rocha, R. Mendes, M. P. F.-Garcia, A. Guedes, P. B. Tavares, J.-M. Grenèche, J. P. Araújo and C. Freire, Superparamagnetic MFe_2O_4 (M = Fe, Co, Mn) Nanoparticles: Tuning the Particle Size and Magnetic Properties through a Novel One-Step Coprecipitation Route, *Chem. Mater.*, 2012, **24**, 1496-1504.
17 D. Carta, M. F. Casula, P. Floris, A. Falqui, G. Mountjoy, A. Boni, C. Sangregorio and A. Corrias, Synthesis and microstructure of manganese ferrite colloidal nanocrystals, *Phys. Chem. Chem. Phys.* 2010, **12**, 5074-5083.
18 L. I. Cabrera, A. Somoza, J. F. Marco, C. J. Serna and M. P. Morales, Synthesis and surface modification of uniform MFe_2O_4 (M = Fe, Mn, and Co) nanoparticles with tunable sizes and functionalities, *J. Nanoparticle Res.*, 2012, **14**, 1-14.
19 H. Yang, C. Zhang, X. Shi, H. Hu, X. Du, Y. Fang, Y. Ma, H. Wu and S. Yang, Water-soluble superparamagnetic manganese ferrite nanoparticles for magnetic resonance imaging, *Biomaterials*, 2010, **31**, 3667-3673.
20 J. Lu, S. Ma, J. Sun, C. Xia, C. Liu, Z. Wang, X. Zhao, F. Gao, Q. Gong, B. Song, X. Shuai, H. Ai and Z. Gu, Manganese ferrite nanoparticle micellar nanocomposites as MRI contrast agents for liver imaging, *Biomaterials*, 2009, **30**, 2919-2928.
21 A. Tomitaka, A. Hirukawa, T. Yamada, S. Morishita and Y. Takemura, Biocompatibility of various ferrite nanoparticles evaluated by in vitro cytotoxicity assays using HeLa cells, *J. Magn. Magn. Mater*., 2009, **321**, 1482-1484.
22 S. Dandamudi and R. B. Campbell, Development and characterization of magnetic cationic liposomes for targeting tumor microvasculature, *Biochim. Biophys. Acta*, 2007, **1768**, 427-438.
23 A. Akbarzadeh, M. Samiei and S. Davaran, Magnetic nanoparticles: preparation, physical properties, and applications in biomedicine, *Nanoscale Res. Lett.,* 2012, **7**, 144-157.
24 M.-J. R. P. Queiroz, R. C. Calhelha, L. Vale-Silva, E. Pinto and M. S.-J. Nascimento, Novel [6-(hetero)arylamino]thieno[3,2-*b*]pyridines: synthesis and antitumoral activities, *Eur. J. Med. Chem.,* 2010, **45**, 5732-5738.
25 J. M. H. Kremer, M. W. J. v. d. Esker, C. Pathmamanoharan and P. H. Wiersema, Vesicles of variable diameter prepared by a modified injection method, *Biochemistry*, 1977, **16**, 3932-3935.
26 A. R. O. Rodrigues, I. T. Gomes, B. G. Almeida, J. P. Araújo, E. M. S. Castanheira and P. J. G. Coutinho, Magnetoliposomes based on nickel ferrite nanoparticles for biomedical applications, *Phys. Chem. Chem. Phys.*, 2015, **17**, 18011-18021.
27 C.N.C. Costa, A.C.L. Hortelão, J.M.F. Ramos, A.D.S. Oliveira, R.C. Calhelha, M.-J.R.P. Queiroz, P.J.G. Coutinho and E.M.S. Castanheira, A new antitumoral Heteroarylaminothieno[3,2-*b*]pyridine derivative: its incorporation into liposomes and interaction with proteins monitored by fluorescence, *Photochem. Photobiol. Sci.,* 2014, **13**, 1730-1740.
28 Y. Tamba, H. Terashima and M. Yamazaki, A membrane filtering method for the purification of giant unilamellar vesicles, *Chem. Phys. Lipids*, 2011, **164**, 351-358.
29 T. Tanaka, Y. Tamba, S. M. Masum, Y. Yamashita and M. Yamazaki, La^{3+} and Gd^{3+} induce shape change of giant unilamellar vesicles of phosphatidylcholine, *Biochim. Biophys. Acta*, 2002, **1564**, 173-182.
30 B. Valeur, Molecular Fluorescence – Principles and Applications, Wiley-VCH, Weinheim, 2002.
31 J. N. Demas and G. A. Crosby, The measurement of photoluminescence quantum yields. – Review, *J. Phys. Chem*., 1971, **75**, 991-1024.
32 S. Fery-Forgues and D. Lavabre, Are fluorescence quantum yields so tricky to measure? A demonstration using familiar stationery products, *J. Chem. Educ.*, 1999, **76**, 1260-1264.
33 I. Johnson and M. T. Z. Spence, Molecular Probes Handbook: A Guide to Fluorescent Probes and Labeling Technologies, 11th Ed., Invitrogen, 2011.
34 A. R. O. Rodrigues, I. T. Gomes, B. G. Almeida, J. P. Araújo, E. M. S. Castanheira and P. J. G. Coutinho, Magnetoliposomes based on nickel/silica core/shell nanoparticles: synthesis and characterization, *Mat. Chem. Phys.*, 2014, **148**, 978-987.
35 A. S. Edelstein and R. C. Cammaratra, *Nanomaterials: Synthesis, Properties and Applications*, Taylor & Francis Group, New York, 1996.
36 C. Dong, G. Wang, D. Guo, C. Jiang and D. Xue, Investigation of the thermal stability of Mn ferrite particles synthesized by a modified co-precipitation method, *Sci. China Phys. Mech. Astron.,* 2013, **56**, 568-572.
37 O. Stenzel, The Physics of Thin Film Optical Spectra – An Introduction, Springer, Berlin, 2005.
38 M. Y. Rafique, P. Li-Qing, Q. Javed, M. Z. Iqbal, Q. Hong-Mei, M. H. Farooq, G. Zhen-Gang and M. Tanveer, Growth of monodisperse nanospheres of $MnFe_2O_4$ with enhanced magnetic and optical properties, *Chinese Phys. B,* 2013, **22**, article 107101.
39 D. L. Schulz, R. A. Sailer and A. N. Caruso, Superparamagnetic Transition Metal Iron Oxygen Nanoparticles, *US Patent No. 0194733* (2009).

40 L. Khanna and N. K. Verma, Synthesis, characterization and in vitro cytotoxicity study of calcium ferrite nanoparticles, *Mater. Sci. Semicond. Process.*, 2013, **16**, 1842-1848.
41 B. D. Cullity and C. D. Graham, *Introduction to Magnetic Materials*, John Wiley & Sons Inc., Hoboken, New Jersey (USA), 2009.
42 D. R. Lide, Ed., *CRC Handbook of Chemistry and Physics*, 89th Ed., CRC Press/Taylor and Francis, Boca Raton, FL, USA, 2009,
43 M.-J. R. P. Queiroz, S. Dias, D. Peixoto, A. R. O. Rodrigues, A. D. S. Oliveira, P. J. G. Coutinho, L. A. Vale-Silva, E. Pinto and E. M. S. Castanheira, New potential antitumoral di(hetero)-arylether derivatives in the thieno[3,2-*b*]pyridine series: Synthesis and fluorescence studies in solution and in nanoliposomes, *J. Photochem. Photobiol. A: Chem.*, 2012, **238**, 71-80.
44 P. Pradhan, J. Giri, R. Banerjee, J. Bellare and D. Bahadur, Preparation and characterization of manganese ferrite-based magnetic liposomes for hyperthermia treatment of cancer, *J. Magn. Magn. Mater.*, 2007, **311**, 208-215.
45 G. Hungerford, E. M. S. Castanheira, M. E. C. D. Real Oliveira, M. G. Miguel and H. D. Burrows, Monitoring ternary systems of $C_{12}E_5$/water/tetradecane via the fluorescence of solvatochromic probes, *J. Phys. Chem. B*, 2002, **106**, 4061-4069.
46 P. Greenspan and S. D. Fowler, Spectrofluorometric studies of the lipid probe, Nile Red, *J. Lipid Res.*, 1985, **26**, 781-789.
47 I. and G. Krishnamoorthy, Probing the link between proton transport and water content in lipid membranes, *J. Phys. Chem. B*, 2001, **105**, 1484-1488.
48 P. J. G. Coutinho, E. M. S. Castanheira, M. C. Rei and M. E. C. D. Real Oliveira, Monitoring ternary systems of $C_{12}E_5$/Water/Tetradecane via the fluorescence of solvatochromic probes, *J. Phys. Chem. B*, 2002, **106**, 12841-12846.
49 E. Feitosa, F. R. Alves, A. Niemiec, M. E. C. D. R. Oliveira, E. M. S. Castanheira and A.L.F. Baptista, Cationic liposomes in mixed didodecyl-dimethylammonium bromide and dioctadecyldimethylammonium bromide aqueous dispersions studied by differential scanning calorimetry, Nile Red fluorescence, and turbidity, *Langmuir,* 2006, **22**, 3579-3585.
50 S. Zhang, H. Niu, Y. Zhang, J. Liu, Y. Shia, X. Zhang and Y. Cai, Biocompatible phosphatidylcholine bilayer coated on magnetic nanoparticles and their application in the extraction of several polycyclic aromatic hydrocarbons from environmental water and milk samples, *J. Chromatogr. A*, 2012, **1238**, 38-45.
51 S. García-Jimeno, E. Escribano, J. Queralt and J. Estelrich, Magnetoliposomes prepared by reverse-phase followed by sequential extrusion: Characterization and possibilities in the treatment of inflammation, *Int. J. Pharmaceut.,* 2011, **405**, 181-187.
52 H. Curtis and N. Barnes, *Biology*, 5th Edition, Worth Publishers, New York, 1989.

GRAPHICAL ABSTRACT

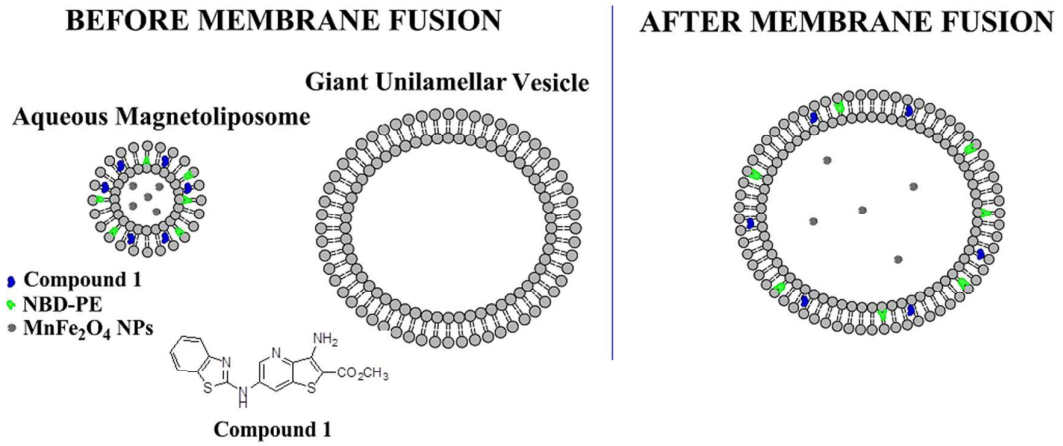

Aqueous and solid magnetoliposomes containing $MnFe_2O_4$ nanoparticles were prepared and evaluated as nanocarriers for a new antitumor drug.